RE-IMPLEMENTATION AND CHARACTERIZATION OF SJÖBO DRY SAND IN OPENRADIOSS: IMPROVING GROUND SHOCK PREDICTIONS THROUGH TRI-AXIAL AND WAVE VELOCITY TESTING

Leo Laine[a] and Ola Pramm Larsen[b]

[a]LL Engineering AB, Sjupundsgatan 41, 414 84 Göteborg, Sweden,
e-mail: leo.laine@telia.com, webpage: http://www.l2e.se,

[b]CAEWIZ Consulting A/S, Grinda 2B, 0861 OSLO, Norway,
email: ola.pramm.larsen@caewiz.no

Keywords: Ground shock, Dry Sand, Mechanical Properties of Dry Sand, Compaction Equation of State, Shear Strength Model, Shock Waves in Sand, OpenRadioss

Abstract

This paper presents the re-implementation of a well-established compaction and shear strength model, originally available in AUTODYN and widely cited in the literature, into OpenRadioss, an open-source explicit solver for broad range of applications, including shock and impact simulations. The objective is to enhance ground shock predictions by accurately capturing the compaction behavior and shear strength of dry sand. The study focuses on Sjöbo sand, a well-characterized quartz sand, with mechanical properties determined through triaxial compression tests under isotropic consolidation. A porous equation of state (EOS) was developed based on volumetric compression data, while shear wave and longitudinal wave velocity measurements provided estimates of bulk sound speed and shear modulus over a range of pressures. The in situ dry density of the sand was approximately 1574 kg/m³, with an average water content of 6.57%. The re-implementation ensures consistency with previous AUTODYN models while leveraging OpenRadioss' open-source capabilities for broader accessibility and further development. An improved approach for interpolating the unloading behavior from compaction curves was incorporated, ensuring accurate energy dissipation in high-pressure release scenarios. The implementation is validated through single-element tests and particle velocity impact simulations, providing a benchmark for further studies on granular materials under dynamic loading. As a successor to previous research efforts, this work aims to support the OpenRadioss community by providing a validated dry sand material model, enhancing the simulation of granular materials and facilitating further development in open-source computational mechanics.

1 INTRODUCTION

Accurate prediction of ground shock wave propagation and attenuation is critical in many engineering applications, including the design of protective structures, assessment of conventional weapon effects, and evaluation of buried explosions. The mechanical properties of granular materials, such as sand, strongly influence shock behavior. In 2001, Laine and Sandvik introduced the Sjöbo sand model [1], which provided an experimentally validated framework for characterizing sand behavior under dynamic loading. Its subsequent implementation in AUTODYN became a widely adopted approach in the field.

Since its initial publication of the material properties for dry sand [1], the Sjöbo sand model continues to be referenced, in recent studies (2023–2025), for example in [2] applied FEM tools to implement dynamic replacement of soft soils, while in [3] evaluated damage in fiberboard boxes during vertical impact tests. In [4] developed a state equation model incorporating pressure wave propagation speed during high-speed projectile impacts in sand, and [5] validated numerical models of explosive ground shock propagation in dry sand with digital image correlation. Further studies by [6]- 12 have extended the model's applicability and enriched our understanding of granular material behavior under dynamic loading conditions.

This paper presents the re-implementation of the Sjöbo sand model within OpenRadioss, an open-source explicit solver for shock and impact simulations [18]. By transitioning this well-established model to an open-source platform, we aim to provide a robust and accessible tool for the shock and blast community. The current study focuses on validating the re-implementation through single-element tests and particle velocity impact experiments, ensuring that the model accurately captures the compaction behavior and shear strength of dry sand.

The paper is organized as follows: Section 2 reviews the original mechanical properties derived for dry sand (2001) [1]. Section 3 discusses the re-implementation of the compaction EOS for the dry sand model within OpenRadioss and explains how the compaction EOS and unloading phase can be modified to reduce energy dissipation. Section 4 describes the re-implementation of the shear strength model. Section 5 presents simple validation tests using single 3D solid element simulations. Section 6 discusses the challenges of modeling ground shock in both near-field and far-field conditions. Finally, Section 7 provides conclusions and outlines future research directions for improving ground shock predictions using the Sjöbo sand model.

2 ORIGINAL MECHANICAL PROPERTIES DERIVED FOR DRY SAND (2001)

2.1 Original tri-axial tests

The Norwegian Geotechnical Institute (NGI) have both characterized the soil and performed triaxial tests on the sand from Sjöbo, Sweden [14]. Different isotropic and deviatoric stress loading conditions were conducted, during the different tri-axial stress states longitudinal- and shear waves were measured in the sand with piezoelectric sensors, which characterized the bulk sound speed for different densities.

2.2 Characterization of soil

The grain size distribution in the sand was medium to coarse, with grain size number C60/C10 approximately equal to 2. The content of organic compounds was less than one percent. The in situ dry density was approximately 1574 [kg/m^3]; the average water content was approximately 6.57 percent. Finally, the average specific weight of the grains was 2641 [kg/m^3] [13]. It is important to note that the material model data is valid for dry sand

conditions, with the in situ dry density and average water content expressed in this section.

2.3 Original Mechanical Properties derived in 2001 paper

Following mechanical properties were derived from the NGI experiments in the original paper, see Fig. 1. Top left subplot shows compaction Equation of State (EOS), with linear unloading bulk modulus, which is calculated by the bulk sound speed c_i, $K_u = \rho_i \cdot c_i^2$, see top right plot in Fig. 1. Bottom left plot in Fig 1. shows the shear strength model as a function of pressure, which uses the shear modulus defined in bottom right corner in Fig 1.
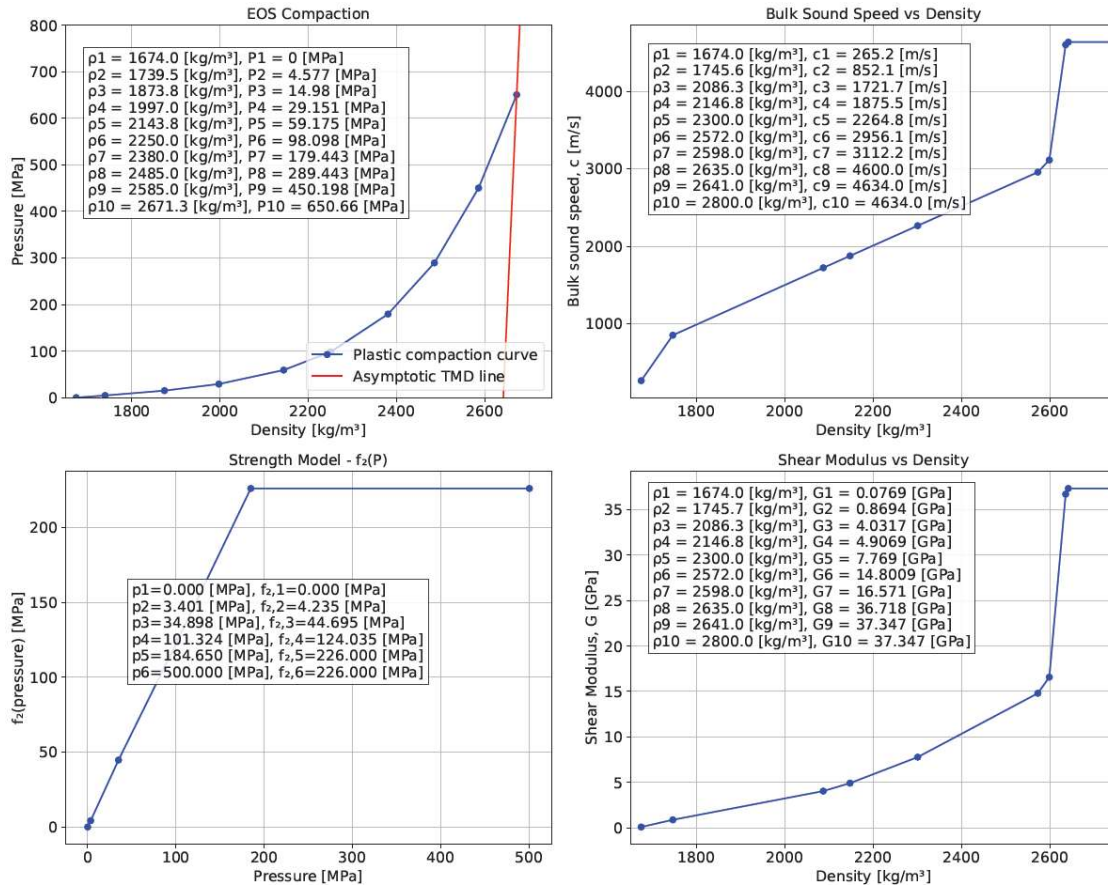
Figure 1. Original Mechanical Properties derived for Dry Sand from Sjöbo Sweden [1]. Yield surface is defined as $f_2(P)$.

3 RE-IMPLEMENTATION OF COMPACTION EOS

3.1 Compaction EOS with density dependent unloading bulk modulus

The plastic compaction curve is given as a 10 point piecewise linear curve, namely pressure as function of density $P_i(\rho_i)$, where the points below 60 MPa pressure was derived from the tri-axial tests [13]. The plastic compaction curve for pressures above 60 [MPa] was predicted by using a polynomial best fit of fifth order, see Fig 1 top left plot. The Theoretical Maximum Density (TMD) was set equal to the average specific weight of the grains in the sand, $\rho_{TMD} = 2641$ [kg/m^3]. The solid "asymptotic TMD line" to this curve is linear:

$$P(\rho = \rho_{TMD}) = 0 \tag{1}$$

$$P = c_s^2 \rho_{TMD} \cdot \mu \quad \text{with} \quad \mu = \rho/\rho_0 - 1 \text{ and} \quad \rho \geq \rho_{TMD} \tag{2}$$

where ρ_{TMD} is the TMD density where no porosity is left, and c_s is the bulk sound speed of fully compacted solid material. The mineral content in the sand is similar what would be found in granite, thus the bulk sound speed of fully compacted material was derived from Shock Hugoniot Data for Westerly Granite [16]. The $c_s = 4636$ [m/s] value was given by the two states ($\rho_0 = 2627$ [kg/m³], $P_0 = 0$) and ($\rho_1 = 3530$ [kg/m³], $P_0 = 19.394$ [GPa]).

In the original model, the elastic unloading wave velocity c_i was based upon Pressure(P)-wave v_p and Shear(S)-wave v_s velocity measurements [1] and [13]. The bulk sound speed can be calculated by

$$c = \sqrt{\left(v_p^2 - \frac{4}{3}v_s^2\right)} \tag{3}$$

In Fig. 6 the measured P-wave and S-wave velocities for the dry sand are shown together with the calculated bulk sound speed c_i.
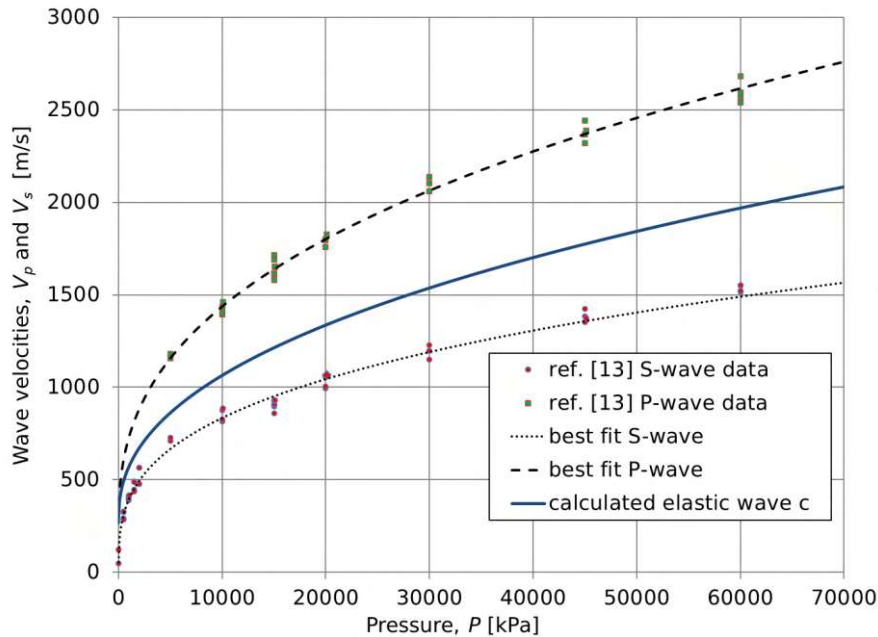

Figure 2. Measured pressure and shear wave velocities as a function of pressure for dry sand (Sjöbo). The blue line corresponds to calculated bulk sound speed c_i, from [1] and [13].

The longitudinal and shear wave velocities above the density 2150 [kg/m³] were predicted by using linear approximation. The elastic unloading/re-loading compaction curve is given by the density dependent unloading bulk modulus $K_u = c_i^2(\rho_i) \cdot \rho_i$. In the material input the bulk sound speed is given as function of density as piecewise linear 10 points, $c_i(\rho_i)$, see Fig 1 top right plot.

A new feature has been introduced in the compaction EOS, allowing for different reloading response when the sand material expands back to its original volume. The model provides two reloading options: (0) the material follows the zero-pressure line until it reaches the most recent elastic unloading slope used, or (1) plastic compaction pressure reoccurs, treating the expanded material as virgin sand. This functionality is controlled by the Plastic Compaction Re-loading ON (PLACOREON) option in the input file, where PLACOREON = 0 disables plastic reloading and PLACOREON = 1 enables it.

3.2 Energy dissipation during shock propagation in dry sand during unloading

One of the most important effects when studying buried detonation of explosives and the ground shock propagation in far-field, i.e. scaled distances higher than D > 1 [m/kg$^{1/3}$] for TNT, is the fact that soils such as dry sand is compacted by the shock wave propagated in the surrounding media. If the compaction effect is too large during the unloading phase, the shock wave energy from the explosive is dissipated too fast which give a false low loading on buried structures. Therefore it is proposed that the unloading phase in EOS is given more modelling focus and that the unloading bulk sound speed is made not only density dependent $c_i(\rho_i)$ as top right plot in Fig. 1, but also make the bulk sound speed unloading pressure dependent, $c_i(\rho_i, P_u)$. This is in fact supported by just studying the mechanical isotropic loading and unloading during the tri-axial isotropic pressure loading and unloading conducted by NGI, see Fig. 3. For example, if the unloading curves from pressure 15 MPa, is followed towards pressures close to zero pressure, it is evident that the unloading bulk modulus is not only dependent on density but also the unloading pressure.
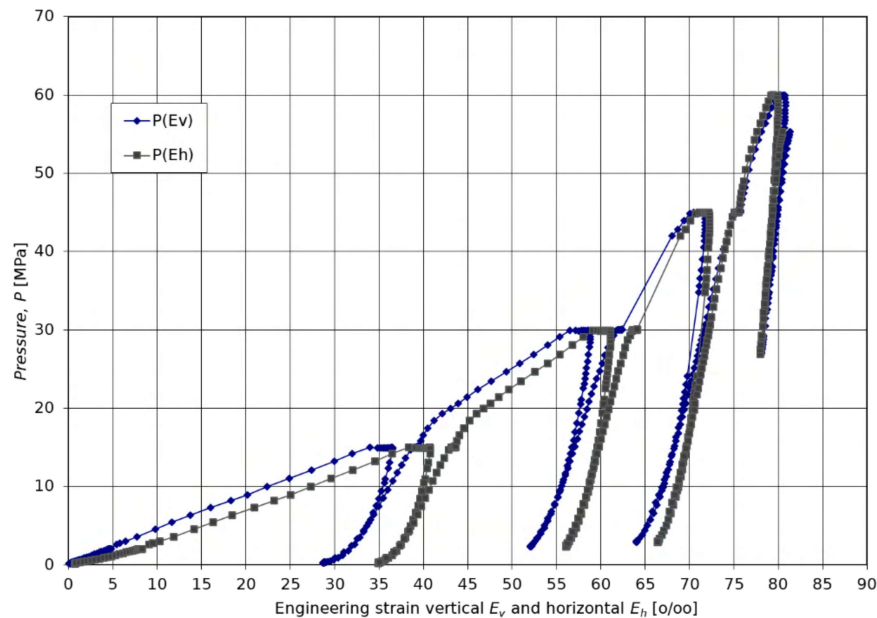
Figure 3. Pressure as a function of vertical and horizontal engineering strain, [14].

In year 2012, authors showed a proposal of how the EOS unloading phase could be modified and include the behavior seen in Fig. 3 for low unloading pressures and conducted implementation into user subroutine in AUTODYN [14], more details can be found in [15] which also includes an appendix with code.

The implemented compaction EOS in OpenRadioss is aimed to have two versions of unloading, the original version 2001, which matches with the Autodyn implementation, see section 2.3 which is in default given with derived mechanical properties of the dry sand, see Fig 1. The second unloading is the improved version from year 2012 with density and pressure dependent unloading bulk sound speed $c_i(\rho_i, P_u)$, see [14],[15].

3.3 Compaction EOS with density and pressure dependent unloading bulk modulus

As originally proposed in [14], the main input to the modified EOS uses three piece wise linear curves. The first one is the plastic compaction curve $P_c(\rho)$, see Fig. 5. The second piecewise linear input is the initial wave velocity $c_b(\lambda)$, where $\lambda = \rho(P = 0)$. The third piece wise linear input is how curved the unloading is along the density axis when the pressure is equal to zero $\gamma(\lambda)$, here named curve factor.

The unloading is described with following two equations

$$c_b(\lambda)^2 = \frac{P_c(\lambda + \rho_L(\lambda))}{\rho_L(\lambda)} \tag{4}$$

and

$$P_{\text{UL}}(\rho) = \frac{P_c(\lambda + \rho_L(\lambda))}{e^{\gamma(\lambda)} - 1} \left(e^{\frac{\gamma(\lambda)}{\rho_L(\lambda)}(\rho - \lambda)} - 1 \right) \tag{5}$$

where λ is the density in the $\rho - P$ space along the $P = 0$ line, $\rho_L(\lambda)$ is in ρ space and is defining the horizontal distance for an unloading or re-loading curve, according to Fig. 4. The equations (4) and (5) describes the relationship between the ρ space and the wave velocity c_b. Some of the main properties for the $P_{UL}(\rho)$ equation (5) is that when the density is on its initial or final values it becomes

$$P_{\text{UL}}(\rho = \lambda) = 0 \tag{6}$$

and

$$P_{\text{UL}}(\rho = \lambda + \rho_{\text{L}}(\lambda)) = P_c. \tag{7}$$
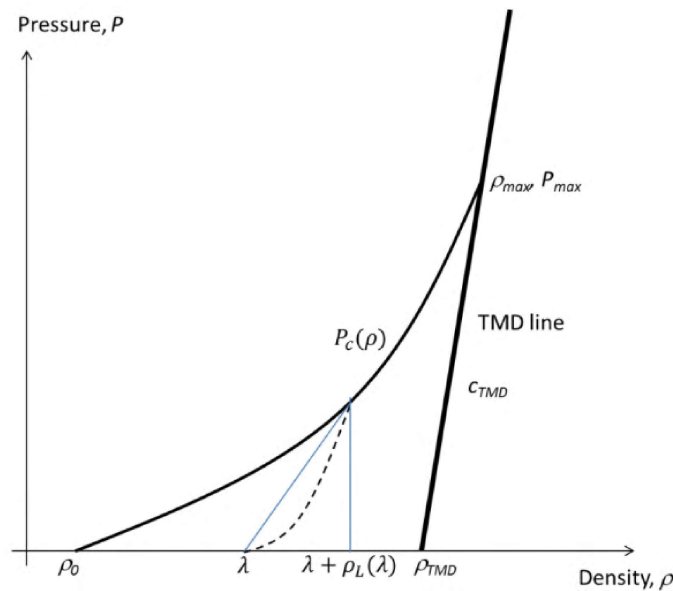
Figure 4. Shows the plastic compaction curve $P_c(\rho)$, Theoretical Maximum Density (TMD) line, the intersection of arbitrary unloading curve with the $P = 0$ line λ, and the density span of unloading curve $\rho_L(\lambda)$.

Fig. 4. Shows the plastic compaction curve $P_c(\rho)$, Theoretical Maximum Density (TMD) line, the intersection of arbitrary unloading curve with the $P = 0$ line λ, and the density span of

unloading curve $\rho_L(\lambda)$.

Another main property is how the curving of the unloading is treated in between the initial and end value. First when the curve factor goes towards zero:

$$\lim_{\gamma(\lambda)\to 0} P_{UL}(\rho) = \frac{P_c(\lambda+\rho_L(\lambda))}{\rho_L(\lambda)}(\rho - \lambda) = c_b(\lambda)^2(\rho - \lambda) \tag{8}$$

This means that the unloading becomes the same as in the original model with density dependent elastic unloading. Secondly when the curve factor goes to infinity:

$$\lim_{\gamma(\lambda)\to \infty} P_{UL}(\rho) = \begin{cases} 0 \text{ if } \lambda \le \rho < \lambda + \rho_L(\lambda) \\ P_c(\lambda + \rho_L(\lambda)) \text{ if } \rho = \lambda + \rho_L(\lambda) \end{cases} \tag{9}$$

This will give a flip turned L-shape like unloading curve. This means that equations (4) and (5) are relatively simple but powerful relationship formulation which gives the possibility to define the unloading for the whole $\rho - P$ space by using three independent piece wise linear input data curves $P_c(\rho)$, $c_b(\lambda)$, and $\gamma(\lambda)$.

To illustrate the relationship and how the curve factor $\gamma(\lambda)$ influence the unloading, the unloading shape is shown for $\gamma(\lambda) = 0, 5, \text{ and } 100$, see Fig. 5.
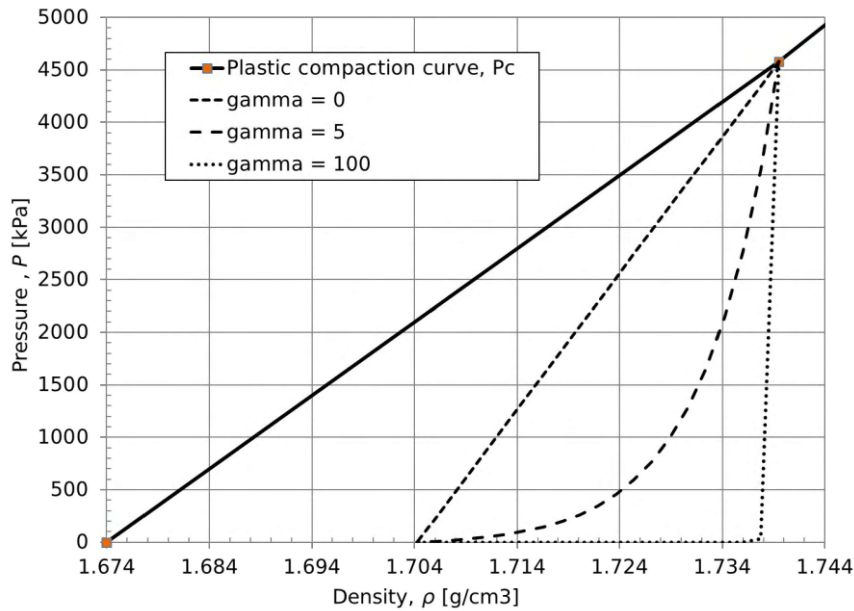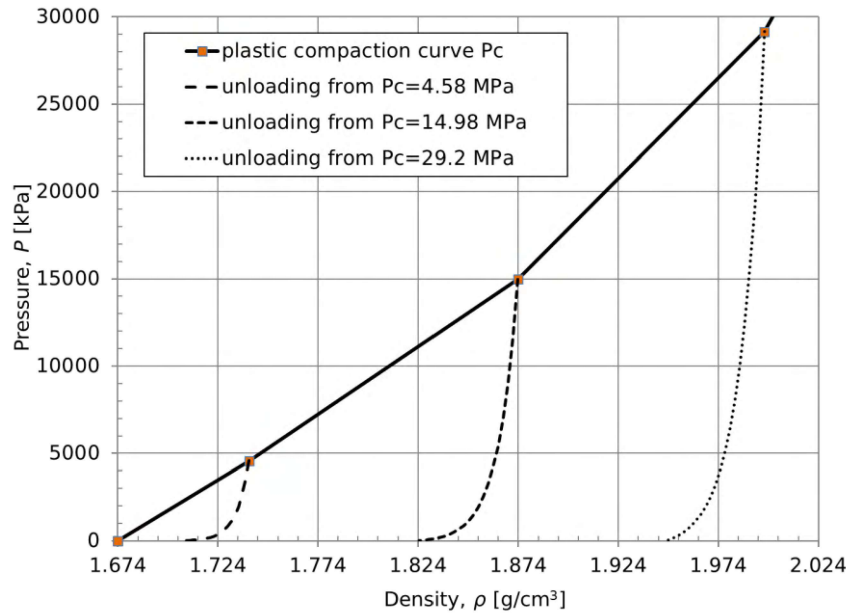

Figure 5. Three different unloading curves depending on the setting of the curve factor $\rho_L(\lambda)$ = 0, 5, and 100, respectively.

3.3 Derived input data for Dry Sand for improved modelling of unloading curves

The derived input data for dry sand is based on fitting the experimental tests from [1] and [13]. The first input is the plastic compaction curve $P_c(\rho)$, which is unchanged input from [1], see Fig. 6. The unloading shape derived from experiments are shown for three different pressure levels, see Fig. 6. The plastic compaction curve is given until it reaches the theoretical maximum density line, see also Fig. 4.

Figure 6. Plastic compaction curve until reaching theoretical maximum density line and unloading curves for three different pressure levels.

In the original model, the elastic unloading wave velocity $c_b(\lambda)$ was based upon wave speed measurements [1] and [13]. In Fig. 3 the measured pressure wave and shear wave for the dry sand is shown. From the measurements the calculated $c_b(\lambda)$ is also shown in Fig. 3. The input data of $c_b(\lambda)$ was modified and instead of using the measured waves the slope of the mechanical unloading curves was used to calculate the initial unloading wave, see Fig. 3.

In Fig. 7 the initial unloading wave $c_b(\lambda)$ is shown for the original model and the modified input. It can be seen that the black curve for the modified input is quite lower for the most part compared with the original model input [1].
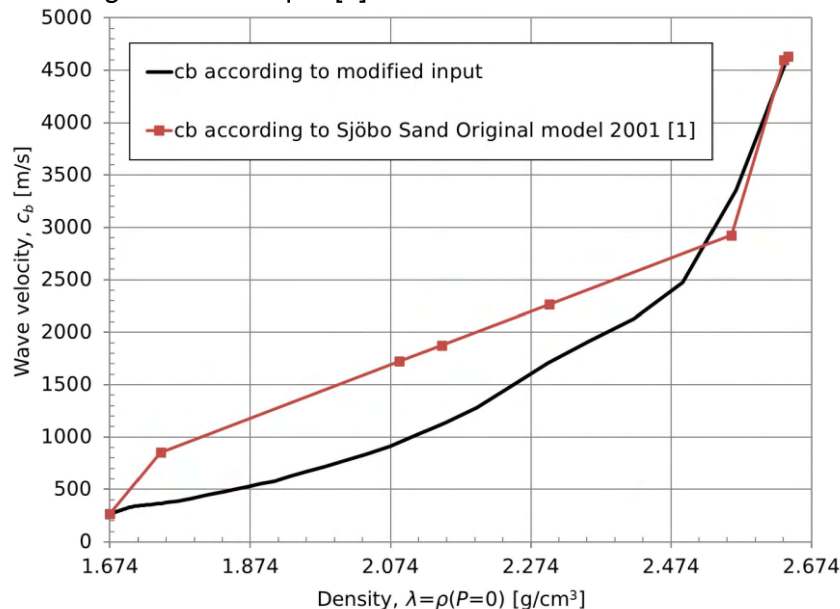

Figure 7. Initial unloading wave velocity $c_b(\lambda)$ as a function of density λ (along $P = 0$ line).

The third input is the curve factor $\gamma(\lambda)$ which defines the shape of the unloading curve. In Fig.

8 the curve factor is given for the modified input and it starts with about 5 to 6 and then decay down to 0 when the theoretical maximum density line is reached. The curve factor has been determined by fitting the experimental results to the model. At the theoretical maximum density line the unloading curve is linear with constant maximum unloading wave velocity.
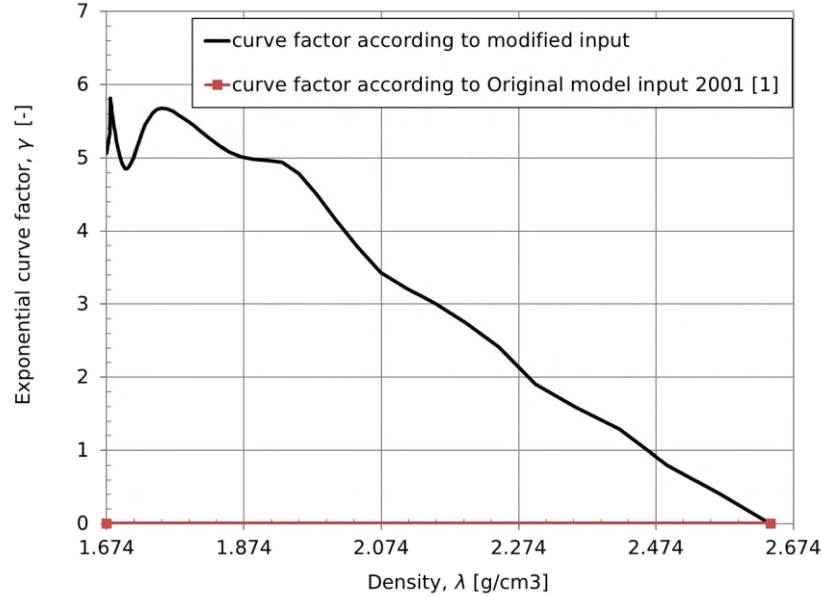
Figure 8. Curve factor $\gamma(\lambda)$ as a function of density λ (along $P = 0$ line).

The unloading curves represent an overall fit with several isotropic compression measurements performed on the dry sand [13]. The input data shown here is just one example of how the EOS model can be used. The implemented EOS model is a powerful way of numerically describe the loading and unloading for numerous soils with different properties of initial density, moisture content, and granularity.

4 RE-IMPLEMENTATION OF SHEAR STRENGTH MODEL

4.1 Density dependent shear modulus
By use of the measured values of the shear wave velocities v_s, see Fig 2, the shear modulus was calculated from

$$G_i = v_s^2 \rho_i \tag{10}$$

Input data for the density dependent shear modulus, G( ), is shown in Fig. 1 bottom right plot. The shear modulus curve is given as 10 point piecewise linear curve, namely shear modulus as function of density $G_i(\rho_i)$.

4.2 Pressure dependent yield surface
The yield surface is defined as pressure dependent and pressure hardening of von Mises type function:

$$Y_i = f_2(P_i) \tag{11}$$

The maximum stress difference from the tri-axial shear tests in [13] were utilized for determination of the maximum yield surface. For pressures above 102 [MPa], a linear approximation was utilized up to a maximum cut off value, which was set equal to the unconfined strength for Peaks Pike Granite [17.]. The yield surface is given by piecewise linear pairs $Y_i(P_i)$. The original data for the yield surface is shown in Fig 1 bottom left plot.

5 USER SUBROUTINE VALIDATION

5.1 Single 3D solid element tests

Single 3D solid element tests were conducted on a 1x1x1 m cube using SI units, with right hand side coordinate system. The first test involved an isotropic compression series to validate the EOS compaction (see Section 5.1). The nodes were constrained in such a way that, as the cube's volume decreased, its shape remained cubic. The second test introduced both shear and compression by applying a vertical velocity to two of the top Z-nodes until the displacement approached the full height of the cube (see Section 5.2). In this second test, all nodes were constrained to prevent horizontal movement, while the other two top Z-nodes were also restricted from vertical displacement. In both test cases, a simulation time of 2 seconds was used. A sandbox containing Python scripts for pre-processing, post-processing, and compiling user subroutines can be found in [19].

5.2 Repeated isotropic compressive displacement and release

The isotropic compressive displacement of the outer top Z-node is shown in Fig. 9 (top left). This figure illustrates multiple loading and unloading cycles, with the cube expanding beyond its original volume at 1.8 s. The top right plot in Fig. 9 depicts the piecewise linear plastic compaction of the EOS, with elastic unloading following a density-dependent slope, as expected. The internal energy levels in Fig. 9 (bottom left) show spikes corresponding to elastic unloading events. Finally, Fig. 9 (bottom right) confirms that no von Mises stresses were introduced during the test.
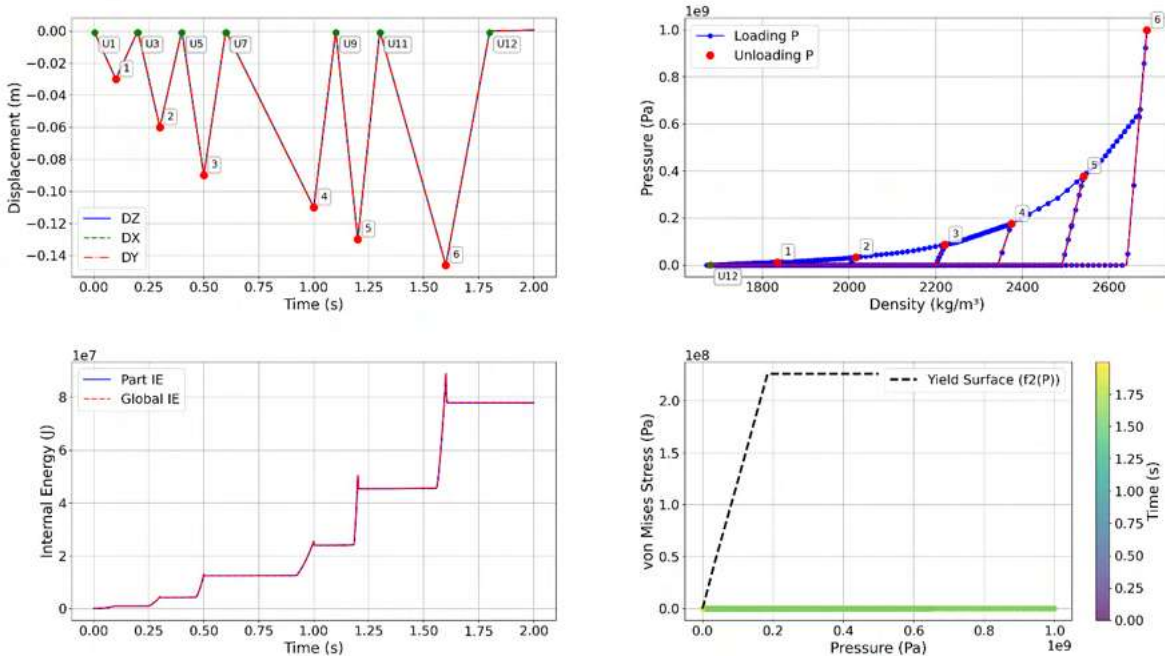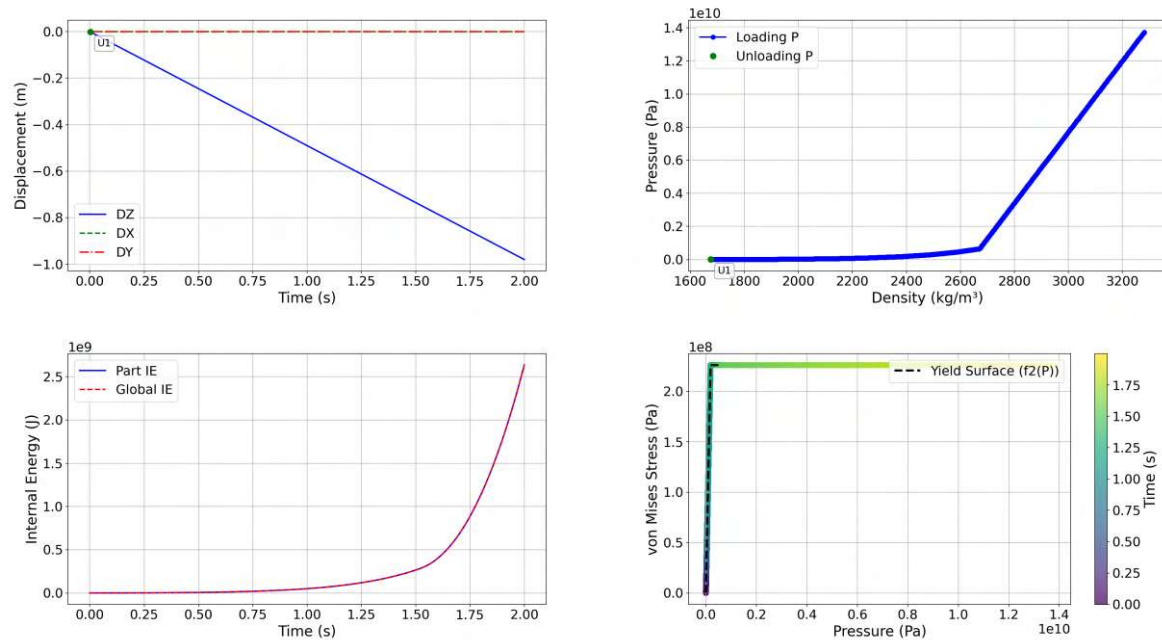

Figure 9. Tri-axial isotropic compression and expansion of single 3D solid element for material model version 2001.

5.3 Constant vertical compressive velocity of two top Z-nodes

The compressive displacement of the 3D solid element under a constant vertical velocity applied to the top two Z-nodes is shown in Fig. 10 (top left). Throughout the simulation, the element undergoes progressive compaction with no unloading phase. The top right plot in Fig. 10 shows the pressure–density response, following the plastic compaction curve of the material model for dry sand. The internal energy (Fig. 10, bottom left) rises steadily as the element absorbs energy during compaction. Meanwhile, the von Mises stress plot (Fig. 10, bottom right) confirms that the test generates both pressure and deviatoric stresses along the

yield surface of the dry sand, as expected under a uniaxial compressive loading condition.

Figure 10. Vertical compressive velocity and expansion of single 3D solid element for material model version 2001.

6   DISCUSSIONS

The experiments in [5] validated numerical modeling of explosive ground shock propagation in dry sand with digital image correlation experiments related to Explosions from Buried Charges. Experiments were thoroughly set up with proper in-situ density and moisture content according to the material properties for dry sand given in [1]. Original dry sand material data from [1] was used and a AUTODYN comparable LS-DYNA model with EOS as EOS_TABULATED_COMPACTION with the possibility to include density dependent unloading bulk modulus $K(\rho)$ and shear strength model MAT_PSEUDO_TENSOR were parameterized. The scenario is having the full complexity of confined buried structure, where the Scaled Stand Off Distance (SSOD) varied from 0.22. 1.09 to 2.17 m/kg$^{1/3}$ TNT, where at least the SSOD< 1 m/kg$^{1/3}$ results in that the explosive gas expansion and cratering highly effects the buried structural response, which was modelled with ALE techniques in [5]. In [5] it was concluded that the near field case the original model dry sand model captured the midpoint deformation of the buried structure quite well. However, in [5] it was also concluded that far-field prediction of structural response needs further work. This aligns with section 3.1 and that the original model with only density dependent unloading bulk modulus $K(\rho)$ has too high energy dissipation for accurate far-field prediction of structural response, see further [15].

In [9] where experimental and numerical characterization of granular material until shock loading, the original dry sand model in AUTODYN was evaluated with following conclusion "The more sophisticated Model2 (original model) brings in additional physical phenomena of material deformation, such as a density-dependent shear modulus and yield stress. These dissipation phenomena notably improve the replication of the dynamic stress–strain curves". This strengthen the case that shear modulus $G(\rho)$ and bulk modulus $K(\rho)$ needs to be density dependent which is now also available in OpenRadioss as the 2001 model version in AUTODYN.

7 CONCLUSIONS AND FUTURE WORK

7.1 Conclusions

The original sand model from 2001 with compaction EOS and shear strength model, with dry sand input parameters, has been successfully implemented as a user subroutine in OpenRadioss. Both the bulk unloading modulus, $K(\rho)$, and the shear modulus, $G(\rho)$, are density-dependent. The default material data found in [1] adequately represents dry sand, provided that the in-situ density and moisture content remain consistent between experiments and simulations. The original model used 10 point pair data input, which still are used for original model data from 2001, however the OpenRadioss allows flexible number of inputs when defined as functions.

In addition, a new feature has been introduced, enabling the dry sand to undergo plastic compaction reloading when it expands back to a larger volume during simulation. This functionality is controlled by the PLACOREON option within the compaction EOS. This means that if the sand returns to its original volume, it will re-compact along the plastic compaction curve. This capability is particularly critical for buried structures that must withstand multiple loading scenarios, such as repeated buried explosions occurring in sequence, accompanied by cratering phenomena near the structure.

7.2 Future work

The next step is to implement the 2012 version of the EOS unloading formulation, incorporating an unloading bulk modulus, that depends on both density and pressure. This modification is crucial for minimizing excessive energy dissipation during ground shock propagation in dry sand, particularly for far-field applications (SSOD > 1 m/kg$^{1/3}$) [15].

Additionally, there may be a need to model shear strength using a shear modulus, $G(\rho, P)$, that is also dependent on both density and pressure. However, further analysis is required to confirm its necessity. This can be achieved through comparisons with elastic longitudinal and shear wave measurements, as conducted in the original experiments [13], and by evaluating its potential benefits in real shock experiments, such as those reported in [9].

ACKNOWLEDGEMENTS

REFERENCES

[1] Laine L. and Sandvik A.(2001), "Derivation of mechanical properties for sand", 4 th Asian-Pacific conference on Shock and Impact Loads on Structures, CI-Premier PTE LTD, vol. 4, pp 353-360, Singapore, https://www.msb.se/siteassets/dokument/ amnesomraden/krisberedskap-ochciviltforsvar/befolkningsskydd/skyddsrum/ vetenskapliga-artiklar/derivation-of-mechanical-properties-for-sand.pdf.

[2] Elsiwi, W., Gunaratne, M., and Mullins, G. (2023), "Application of FEM tools in efficient field implementation of dynamic replacement of soft soils", *International Journal of Geomechanics, 23(10)*, DOI: 10.1080/19386362.2023.2264052.

[3] Lengas, N., Johann, S., Kadoke, D., Müller, K., and Steuernagel, L. (2023), "Damage

assessment of complete, filled fiberboard boxes in regulative vertical impact tests by dropping", *Materials Today: Proceedings, Volume 93, Part 4, 2023, Pages 669-679,* DOI: https://doi.org/10.1016/j.matpr.2023.04.679.

[4] Zhang, K., Kinchi, M., & Watanabe, K. (2023), "Development of an Equation of State Model Considering Pressure Wave Propagation Velocity in High-Speed Projectile Impact and Penetration into Sand". *M&M2023 Materials Mechanics Conference, Japan Society of Mechanical Engineers (JSME) (in Japanese).* DOI: https://doi.org/10.1299/jsmemm.2023.CL0227.

[5] Waddoups, R., Clarke, S., Curry, R., Tyas, A., and Farrimond, D. (2024), "Validation of numerical modelling of explosive ground shock propagation in dry sand with digital image correlation experiments", *19th International Symposium on Interaction of the Effects of Munitions with Structures (IEMSs19) Bonn, Germany,* https://eprints.whiterose.ac.uk/220880/.

[6] Denefeld, V., and Aurich, H. (2024), "Experimental and numerical investigation on alternatives to sandy gravel", *Defence Technology Vol. 31, Pages 130-141.* DOI: https://doi.org/10.1016/j.dt.2023.06.016.

[7] Liu, Z., Li, X., Zhou, D., Wang, X., and Lu, F. (2024), "Influence of Water Cover on the Blast Resistance of Circular Plates", *Journal of Pressure Vessel Technology, 146(4),* DOI: https://doi.org/10.1115/1.4066807.

[8] Ba, B. P., & Vu, P. V. (2024), "Research on simulation of a bullet skimming the ground by the finite element method", *Journal of Military Science and Technology, vol. 100, no. 100,* DOI: https://doi.org/10.54939/1859-1043.j.mst.100.2024.139-145.

[9] Ruiz-Ripoll, M. L., Riedel, W., Stocchi, A., Bagusat, F., and Mayrhofer, K. U. (2024), " Experimental and Numerical Characterization of Granular Material Under Shock Loading", *Journal of Dynamic Behavior of Materials*, DOI: https://doi.org/10.1007/s40870-024-00428-8

[10] Shi, B., Xu, X., Li, J., Li, G., Li, W., Xu, T., Guo, W., Xing, H., and Zhou, J. (2024). Experimental and numerical study on explosion cratering and coupled ground shock in clay. International Journal of Rock Mechanics and Mining Sciences, 173, 105579.

[11] Zhao, Z., Gao, W., Ren, J., Lan, Z., Zhang, Z., Gao, H., He, C., and Zhang, Q. (2025)," Surface-covering water significantly amplifies the explosion impulse of shallow buried explosives", *Defence Technology, In Press, Journal Pre-proof,* DOI: https:doi.org/10.1016/j.dt.2025.01.007

[12] Qin, F., Gao, C., Kong, X., and Yang, Y. (2025), "A new composite protective structure based on the controllability of blast load on the structure layer (Ⅱ): influence factors and design concept", Explosion and Shock Waves, Vol. 45, page 1-12, DOI: 10.11883/bzycj-2023-0463.

[13] Heyerdahl H., Madshus C.(2000), *EOS-data for sand, Triaxial tests on sand from Sjöbo*, Norwegian Geotechnical Institute, NGI, report nr: 20001157-1, 2000.

[14] Laine L. and Larsen O.P. (2012), "Implementation of Equation of State for Dry Sand in Autodyn", *Proceedings of 83rd Shock and Vibration Symposium, New Orleans, USA*, https://www.msb.se/siteassets/dokument/amnesomraden/krisberedskap-och-civilt-forsvar/befolkningsskydd/skyddsrum/vetenskapliga-artiklar/implementation-of-equation-of-state-for-dry-sand-in-autodyn.pdf.

[15] Laine L. (2012), Ground shock, *Markstötvåg*, (in Swedish), Report nr MSB344, 2020-09-28 revision 2, Myndigheten för Samhällsskydd och beredskap, 308p, Karlstad, Sweden, https://www.msb.se/siteassets/dokument/amnesomraden/krisberedskap-och-civilt-forsvar/befolkningsskydd/skyddsrum/referenslitteratur/markstotvag.pdf.

[16] Marsh S. P.(1980), LASL shock Hugoniot data, University of California Press, https://sgp.fas.org/othergov/doe/lanl/docs1/shd.pdf.

[17] Goodman R. E.(1989), Introduction to Rock Mechanics, 2. Ed., New York, Wiley.

[18] OpenRadioss (2025), website: https://github.com/OpenRadioss/OpenRadioss

[19] Laine L. (2025), SANDBOX – for material modelling of Dry Sand with OpenRadioss and python, DOI: https://doi.org/10.5281/zenodo.15001304